



Published in final edited form as:

*Proc SPIE Int Soc Opt Eng.* 2015 March 1; 9414: 94142Y-. doi:10.1117/12.2081284.

## Context-specific method for detection of soft-tissue lesions in non-cathartic low-dose dual-energy CT colonography

Janne J. Näppi<sup>a</sup>, Daniele Regge<sup>b</sup>, and Hiroyuki Yoshida<sup>a</sup>

<sup>a</sup>3D Imaging Research, Department of Radiology, Massachusetts General Hospital and Harvard Medical School, 25 New Chardon Street, Suite 400C, Boston, MA 02114, USA

<sup>b</sup>Institute for Cancer Research and Treatment, Strada Provinciale 142, IT-10060 Candiolo, Turin, Italy

### Abstract

In computed tomographic colonography (CTC), orally administered fecal-tagging agents can be used to indicate residual feces and fluid that could otherwise hide or imitate lesions on CTC images of the colon. Although the use of fecal tagging improves the detection accuracy of CTC, it can introduce image artifacts that may cause lesions that are covered by fecal tagging to have a different visual appearance than those not covered by fecal tagging. This can distort the values of image-based computational features, thereby reducing the accuracy of computer-aided detection (CADe). We developed a context-specific method that performs the detection of lesions separately on lumen regions covered by air and on those covered by fecal tagging, thereby facilitating the optimization of detection parameters separately for these regions and their detected lesion candidates to improve the detection accuracy of CADe. For pilot evaluation, the method was integrated into a dual-energy CADe (DE-CADe) scheme and evaluated by use of leave-one-patient-out evaluation on 66 clinical non-cathartic low-dose dual-energy CTC (DE-CTC) cases that were acquired at a low effective radiation dose and reconstructed by use of iterative image reconstruction. There were 22 colonoscopy-confirmed lesions 6 mm in size in 21 patients. The DE-CADe scheme detected 96% of the lesions at a median of 6 FP detections per patient. These preliminary results indicate that the use of context-specific detection can yield high detection accuracy of CADe in non-cathartic low-dose DE-CTC examinations.

### Keywords

Computer-aided detection; polyp detection; false-positive reduction; dual-energy CT; noncathartic preparation; virtual colonoscopy

## 1. INTRODUCTION

Colorectal cancer is the third most common cancer in both men and women in the United States, where an estimated 96,830 cases of colon cancer and 40,000 cases of rectal cancer were expected to be diagnosed in 2014.<sup>1</sup> Nevertheless, colorectal cancer would be largely preventable by early detection and removal of its benign precursor lesions. Recently,

computed tomographic colonography (CTC) has been endorsed as a viable option for colorectal screening by the guidelines of the American Cancer Society, U.S. Multi-Society Task Force, and the American College of Radiology.<sup>2</sup>

The laxative bowel preparation that is used by conventional colonoscopy examinations has been recognized as one of the most important barriers of patient adherence to colon examinations. However, with CTC, the use of laxative preparation can be avoided by administration of orally ingested fecal-tagging agents that opacify residual fluid and feces on CTC images, thereby facilitating confident detection of lesions. A recent large-scale study demonstrated that laxative-free preparation in combination with computer-aided detection (CADe) can make CTC examinations easy for patients to tolerate while enabling the detection of polyps 10 mm in size at a sensitivity comparable to that of colonoscopy.<sup>3</sup>

However, the presence of fecal tagging in the colon can produce imaging artifacts that change the visual appearance of adjacent soft tissue on CTC images.<sup>4</sup> Figure 1 shows two examples. In Figure 1a, a polyp that is surrounded by lumen air has the average radiodensity of a soft-tissue lesion. When the same polyp is covered by fecal tagging, its radiodensity is substantially lower due to beam hardening and more indicative of fatty tissue or untagged stool, rather than a soft-tissue lesion. In Figure 1b, the colon wall surrounded by lumen air can be seen in great detail, whereas the colon wall that is covered by fecal tagging has a more unspecific appearance. Such image distortions affect the values of image-based shape and texture features that are used for the detection of lesions, thereby reducing the detection accuracy of CADe.

In this study, we developed an experimental context-specific method which can be used to optimize detection parameters separately for air-filled lumen regions and for lumen regions covered by fecal tagging. In air-filled regions where the image quality is high, lesion candidates can be detected at high sensitivity, whereas in fecal-tagged regions where the image quality is lower, the detection can be performed at high specificity to reduce false-positive (FP) detections. For pilot evaluation, the method was integrated into our previously developed dual-energy CADe (DE-CADe) scheme.<sup>5</sup> The detection performance was evaluated by use of clinical non-cathartic dual-energy CTC (DE-CTC) cases that were acquired at ultra-low radiation dose.

## 2. MATERIALS

Sixty-six patients were prepared for a non-cathartic colorectal examination by oral ingestion of 50 ml of iodinated contrast agent (Gastrografin, Bracco Diagnostics, USA) on the day before and two hours prior to the CT examination. The CTC data were acquired by use of a dual-energy CT scanner (SOMATOM Definition Flash, Siemens Healthcare, Germany) in supine and prone positions at 15 mAs for the 140 kVp scan and at 40 mAs for the 80 kVp scan. The DE-CTC images were reconstructed by use of a sinogram-affirmed image reconstruction algorithm<sup>6</sup> at a 0.6 mm reconstruction interval.

### 3. METHODS

#### 3.1 Pre-processing of the DE-CTC images

After the DE-CTC data acquisition, the dual-energy images are subjected to a dual-energy pseudo-enhancement correction that minimizes pseudo-enhancement within the images while preserving the dual-energy information.<sup>7</sup> Next, a single virtual monochromatic image volume<sup>8, 9</sup> is calculated from the dual-energy data for the colon extraction and for shape-based detection of lesions (Figure 2).

The virtual monochromatic image volume and material-specific images are used to determine the abdominal regions of air, fatty tissue, soft tissue, fecal-tagged regions, and their partial-volume interfaces, for guiding a lumen-tracking method that performs automated extraction of the colonic lumen regions.<sup>10, 11</sup>

#### 3.2 Context-specific detection

To perform context-specific detection, the extracted lumen regions are divided and placed into two separate image volumes. Volume  $V_a$  represents aerated lumen regions, whereas volume  $V_t$  represents lumen regions that are covered by fecal tagging. The volumes are calculated by the mapping of the virtual monochromatic CT values,  $u_m$ , as

$$v_a = \min(u_m, 0 \text{ HU}) \quad (1)$$

and

$$v_t = \max\left(\min\left(-1000 \times \frac{u_m}{200}, 0 \text{ HU}\right), -1000 \text{ HU}\right), \quad (2)$$

where  $v_a$  and  $v_t$  are the CT values of  $V_a$  and  $V_t$ , respectively.

In each volume, the lumen regions of interest (regions of air mapped to  $V_a$  and regions of fecal tagging mapped to  $V_t$ ) contain CT values of air, whereas other regions contain CT values of soft tissue (Figure 3). Therefore, the computation of shape features in the volumes is not distorted by three-material interfaces.<sup>10</sup>

To detect sites of lesion candidates, a thick volumetric target region encompassing the perceived colon surface<sup>12</sup> is calculated independently for both volumes. To exclude the artificial partial-volume region that imitates soft-tissue density between the regions of air and fecal tagging, a partial-volume artifact index (PVAX) feature is calculated as

$$\text{PVAX} = \nabla I_w \nabla I_i, \quad (3)$$

where  $I_w$  and  $I_i$  are the water and iodine images of the dual-energy material decomposition. High values of the PVAX feature indicate artificial partial-volume interface regions that will be excluded from the target region.

The sites of lesion candidates are detected within the target regions by use of their virtual monochromatic CT value and the volumetric shape index (SI) and curvedness (CV) features,  $SI = -\frac{2}{\pi} \arctan \frac{\kappa_{max} + \kappa_{min}}{\kappa_{max} - \kappa_{min}}$  and  $CV = \sqrt{(\kappa_{max}^2 + \kappa_{min}^2)}/2$ , where  $\kappa_{max}$  and  $\kappa_{min}$  are the principal curvatures of the implicit local iso-intensity surface.<sup>13</sup> The regions of detected sites are established by hysteresis thresholding of the feature values. To optimize the detection performance, the smallest detectable sites in  $V_a$  and  $V_t$  can be adjusted by use of the volumetric size parameter thresholds,  $T_a$  and  $T_t$ , respectively. The remaining detected sites are then merged into a single detection volume by mapping from  $V_a$  and  $V_t$  into a single detection volume. The detected sites are categorized into three classes,  $D_a$ ,  $D_t$ , and  $D_m$ , that indicate detections originating from air-filled lumen surfaces, those originating from regions covered by fecal tagging, and those originating simultaneously from both types of regions, respectively.

### 3.3 Classification of lesion candidates

The complete region of a lesion candidate is extracted at each detected site by use of a level-set method.<sup>14</sup> To reduce FP detections, several image-based shape, texture, and dual-energy features are calculated from the virtual monochromatic images and material-decomposition images of the extracted lesion candidates.<sup>5</sup> Based on the available feature values, a random-forest ensemble classifier is used to classify the lesion candidates into true-positive (TP) and FP detections.<sup>15</sup> The FP reduction can be optimized by performing the classification independently on the lesion candidates of  $D_a$ ,  $D_t$ , and  $D_m$ .

### 3.4 Evaluation

The locations of clinically significant polyps (  $\geq 6$  mm in largest diameter) that were confirmed by colonoscopy were correlated with the CTC images by a radiologist. A polyp was considered detected correctly by CADe, if the distance between the mass center of a lesion candidate and a true lesion was within the measured radius of the true lesion at either or both supine and prone CTC images of a patient.

To optimize the context-specific detection, we determined the smallest volumetric size of detected sites in  $V_a$  and  $V_t$  that need to be kept in order to detect all lesions in the CTC data at the image scales of 3 mm, 4 mm, 5 mm, and 6 mm.

For pilot evaluation of the detection performance of the DE-CADe scheme, a leave-one-patient evaluation was performed using the DE-CTC data of the 66 patients. At each leave-one-out iteration, the classification parameters were re-established and the random-forest classifier was re-trained before the testing of the classifier at that iteration. At each iteration, the classification parameters were re-established using the training set by use of a 10-fold leave-group-out cross-validation method that was repeated 3 times, and the parameters that yielded the highest average area under the receiver operating characteristic (ROC) curve were used.

## 4. RESULTS

There were 15 lesions  $\geq 10$  mm in size and 7 lesions 6 – 9 mm in size in 21 patients. For the 66 patients, the average CT dose index per CT scan was 0.95 mGy and the effective dose was 0.75 mSv.

Figure 4a shows an analysis of the smallest detected site that needs to be kept in air-filled lumen regions and in those covered by fecal tagging in order to detect all true lesions. The blue line depicts air-filled lumen regions, and the red line depicts regions covered by fecal tagging. The plot indicates that, to detect all true lesions, the smallest site can be larger in lumen regions covered by fecal tagging than in aerated regions. The precise threshold value depends on the image scale at which the detection is performed.<sup>12</sup> The number of all detected sites was smallest at the image scale of 4 mm.

Figure 4b shows the per-lesion detection result for all lesions (dotted line) and for biopsy-confirmed advanced lesions (17 adenomas, serrated lesions, and carcinomas) in terms of free-response ROC curves. The CADe scheme detected 96% of all lesions at a median of 6 FP detections per patient. For advanced lesions (solid line), the detection sensitivity was 100% for lesions  $\geq 10$  mm at a median of 2 FP detections per patient and 100% for lesions 6 – 9 mm in size at a median of 6 FP detections per patient.

## 5. DISCUSSION

The preliminary results of this study indicate that the use of context-specific detection method can yield high detection accuracy for clinically significant colorectal lesions in non-cathartic low-dose DE-CTC. We divided the lumen regions into those filled with air and those covered by fecal tagging to optimize the detection parameters and to track the origin of the lesion candidates for further analysis. Previous approaches that attempted to divide polyp detections into meaningful categories for dedicated analysis have included the identification of polyps located on folds and those not on folds for polyp detection,<sup>16</sup> and morphological decomposition of the colon for improving the polyp size measurement.<sup>17</sup>

The materials of this study were DE-CTC study cases. Unclearly tagged solid stool has been identified as a significant source of false-negative studies in laxative-free CTC,<sup>3</sup> and the interaction of fecal tagging with air and soft tissue is known to introduce three-material partial-volume artifacts that imitate colorectal lesions, thereby reducing the detection accuracy of conventional CADe.<sup>18</sup> Because at two different energies the CT values of materials with high effective atomic numbers, such as those of iodine and barium that are typically used as fecal-tagging agents, deviate more from linear relationship than do materials with a small atomic number,<sup>19</sup> the use of DE-CTC can provide a potential solution for effective detection of lesions in non-cathartic CTC. Previously, we showed that the use of dual-energy image features improves the detection accuracy of CADe significantly for flat lesions and for small polyps over conventional single-energy CTC.<sup>12, 20, 21</sup>

In recent years, there have been concerns about the potential risks of medical radiation by CT examinations.<sup>22</sup> The iterative image reconstruction algorithm that we used in this study facilitated the use of low effective CT dose without compromising diagnostic image quality.

This pilot study had several limitations. The number of polyps was relatively low, and a majority of the polyps were 10 mm in size. A larger number and larger variety of samples is needed to explore the full potential of the context-specific method. The detection performance of the method should also be compared with those of conventional detection methods.

## 6. CONCLUSIONS

We developed a context-specific method that can be used to optimize CADe parameters for polyp detection in CTC. The method was integrated into our DE-CADe scheme. Pilot evaluation of the detection performance of the resulting DE-CADe scheme with 66 clinical non-cathartic low-dose DE-CTC cases indicated high detection accuracy.

## Acknowledgments

This study was partly supported by the NIH/NCI grants of R03CA182107 (PI: Näppi), R01CA095279 (PI: Yoshida), R01CA166816 (PI: Yoshida), and R03CA156664 (PI: Yoshida). We also thank the Enterprise Research Information Systems Group at Partners Healthcare for high-performance computing facilities and support.

## References

1. ACS. Cancer facts and figures. American Cancer Society; 2014.
2. Levin B, Lieberman D, McFarland B, Smith R, Brooks D, Andrews K, et al. Screening and surveillance for the early detection of colorectal cancer and adenomatous polyps, 2008: a joint guideline from the American Cancer Society, the US Multi-Society Task Force on Colorectal Cancer, and the American College of Radiology. *Gastroenterology*. 2008; 134:1570–95. [PubMed: 18384785]
3. Zalis M, Blake M, Cai W, Hahn P, et al. Diagnostic accuracy of laxative-free computed tomographic colonography for detection of adenomatous polyps in asymptomatic adults: a prospective evaluation. *Ann Intern Med*. 2012; 156:692–702. [PubMed: 22586008]
4. Näppi J, Yoshida H. Adaptive correction of the pseudo-enhancement of CT attenuation for fecal-tagging CT colonography. *Med Image Anal*. 2008; 12:413–26. [PubMed: 18313349]
5. Näppi, J.; Kim, S.; Yoshida, H. Automated detection of colorectal lesions with dual-energy CT colonography. In: van Ginneken, B.; Novak, C., editors. *SPIE Medical Imaging 2012: Computer-Aided Diagnosis*. Vol. 8315. 2012. p. 83150Y1-6.
6. Kalra M, Woisetschläger M, Dahlström N, Singh S, Linblom M, et al. Radiation dose reduction with sinogram affirmed iterative reconstruction technique for abdominal computed tomography. *J Comput Assist Tomogr*. 2012; 36:339–46. [PubMed: 22592621]
7. Näppi J, Tachibana R, Regge D, Yoshida H. Information-preserving pseudo-enhancement correction for non-cathartic low-dose dual-energy CT colonography. *LNCS*. 2014; 8676:159–68.
8. Yu L, Leng S, McCollough C. Dual-energy CT-based monochromatic imaging. *Am J Roentgenol*. 2012; 199:S9–S15. [PubMed: 23097173]
9. Heismann, B.; Schmidt, B.; Flohr, T. *SPIE - The International Society for Optical Engineering*. 2012. Spectral computed tomography.
10. Näppi J, Yoshida H. Fully automated three-dimensional detection of polyps in fecal-tagging CT colonography. *Acad Radiol*. 2007; 25:287–300. [PubMed: 17307661]
11. Näppi, J.; Ryu, Y.; Yoshida, H. *Proc SPIE Medical Imaging: Computer-Aided Diagnosis*. Vol. 9035. SPIE Press; 2014. Progressive region-based colon extraction for computer-aided detection and quantitative imaging in cathartic and non-cathartic CT colonography.
12. Näppi J, Kim S, Yoshida H. Adaptive volumetric detection of lesions for minimal-preparation dual-energy CT colonography. *LNCS*. 2012; 7601:30–9.

13. Yoshida H, Näppi J. Three-dimensional computer-aided diagnosis scheme for detection of colonic polyps. *IEEE Trans Med Imaging*. 2001; 20:1261–74. [PubMed: 11811826]
14. Näppi J, Frimmel H, Dachman A, Yoshida H. Computerized detection of colorectal masses in CT colonography based on fuzzy merging and wall-thickening analysis. *Med Phys*. 2004; 31:860–872. [PubMed: 15125004]
15. Näppi J, Regge D, Yoshida H. Comparative performance of random forest and support vector machine classifiers for detection of colorectal lesions in CT colonography. *Lect Notes Comput Sc*. 2012; 7029:27–34.
16. Franaszek, M.; Summers, R.; Pichardt, P.; Choi, J. *Proc SPIE Medical Imaging 2006: Physiology, Function, and Structure from Medical Images*. Vol. 6143. SPIE Press; 2006. Automatic procedure to distinguish colonic polyps located on fold vs. not on fold.
17. Wang, H.; Li, L.; Han, H.; Song, B.; Wei, X.; Liang, Z. *Proc SPIE Medical Imaging 2006: Computer-Aided Diagnosis*. Vol. 9035. SPIE Press; 2014. Automated polyp measurement based on colon structure decomposition for CT colonography.
18. Näppi J, Yoshida H. Virtual tagging for laxative-free CT colonography: pilot evaluation. *Med Phys*. 2009; 36:1830–8. [PubMed: 19544802]
19. Millner M, McDavid W, Waggener R, Dennis M, Payne W, Sank V. Extraction of information from CT scans at different energies. *Med Phys*. 1979; 6:70–1. [PubMed: 440238]
20. Näppi J, Kim S, Yoshida H. Volumetric detection of colorectal lesions for noncathartic dual-energy computed tomographic colonography. *Conf Proc IEEE Eng Med Biol Soc*. 2012; 2012:3740–3. [PubMed: 23366741]
21. Näppi, J.; Kim, S.; Yoshida, H. Volumetric detection of flat lesions for minimal-preparation dual-energy CT colonography. In: Novak, C.; Aylward, S., editors. *SPIE Medical Imaging 2013: Computed-Aided Diagnosis*. Vol. 8670. 2013. p. 8670Y1-6.
22. Chang K, Yee J. Dose reduction methods for CT colonography. *Abdom Imaging*. 2013; 38:224–32. [PubMed: 23229777]

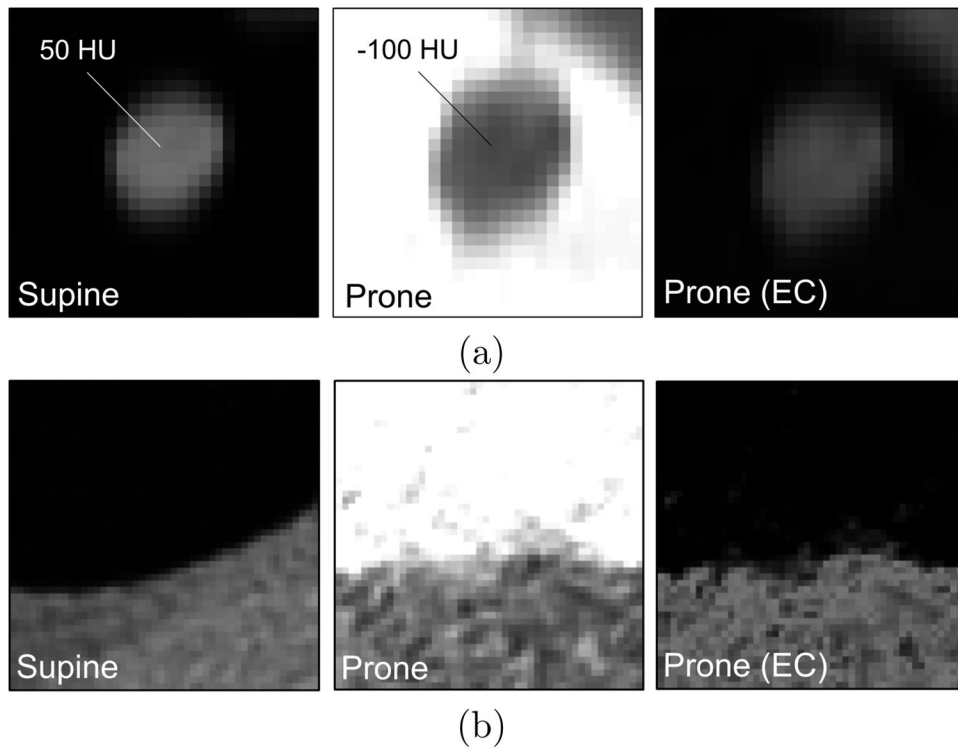


**Figure 1.**

The presence of fecal tagging can affect the visual appearance of adjacent tissue. (a) The CTC image of a 17-mm polyp has a substantially higher average internal radiodensity in supine position where it is surrounded by lumen air, than in prone position where the polyp is covered by fecal tagging. (b) In air-filled lumen regions, colon surface can be visualized in high detail, whereas the colon surface covered by fecal tagging can be distorted by artifacts that complicate confident detection of lesions.



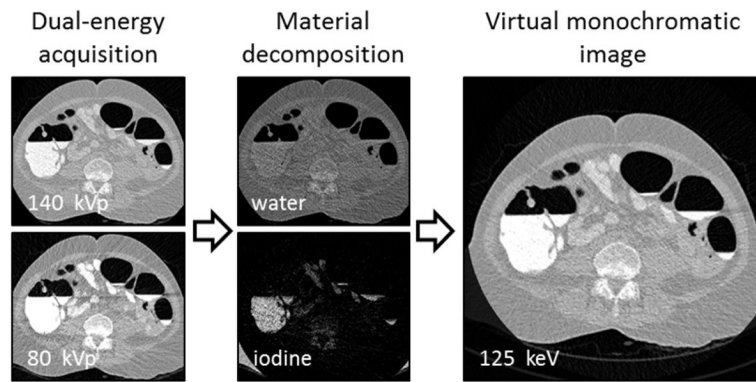


**Figure 2.**

The acquired dual-energy images are decomposed into water and iodine images that are used to synthesize a virtual monochromatic image at a desired energy level.

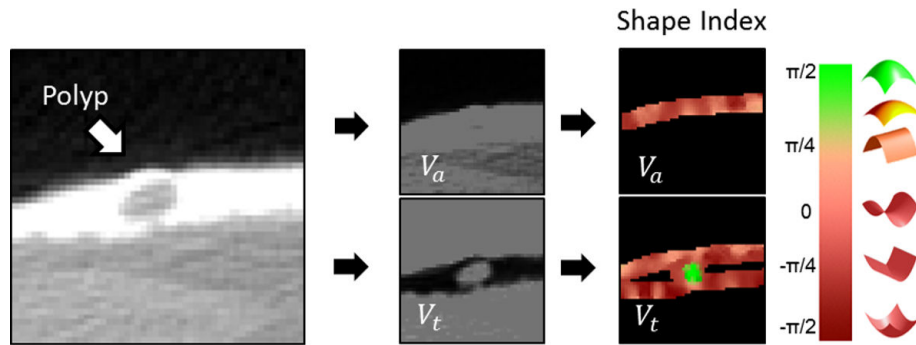


**Figure 3.**

In context-specific detection, the CTC image volume is divided into a separate air-filled lumen image volume ( $V_a$ ) and a lumen image volume that represents regions covered by fecal tagging ( $V_t$ ). The initial detection of suspicious sites is performed independently on both volumes. High values of the SI feature of  $V_t$  (green color) indicate the location of a polyp.

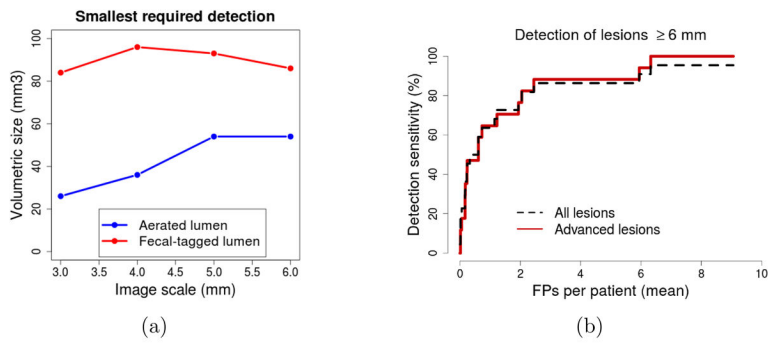


**Figure 4.** (a) An analysis of the smallest detected site in air-filled lumen regions and in those covered by fecal tagging that need to be considered to detect all true lesions. (b) Free-response ROC curves of the detection accuracy of the CAde scheme for all lesions and for advanced lesions.